ACS APPLIED MATERIALS & INTERFACES

Research Article

www.acsami.org

Characteristics of Colored Passive Layers on Zirconium: Morphology, Optical Properties, and Corrosion Resistance

Rebecca J. Holmberg,[†] Sylvain Bolduc,[†] Diane Beauchemin,*[,†] Gregory Jerkiewicz,[†,*] Hubert Schulz,[‡] Ulrich Kohlhaas,[‡] and Henryk Strzelecki[§]

[†]Department of Chemistry, Queen's University, 90 Bader Lane, Kingston, ON, Canada K7L 3N6

[‡]Carl Zeiss Microscopy GmbH, Carl-Zeiss-Strasse 56, 73447 Oberkochen, Germany

[§]Chemical Faculty, Gdańsk University of Technology, 11/12 G. Narutowicza St., 80-233 Gdańsk, Poland

ABSTRACT: Brightly colored and uniform passive layers on Zr can be formed by applying alternating current (ac) voltage (V_{ac}) for 10 s in 10 wt % aqueous Na_2SO_4 solution at T = 298 K. The coloration originating from iridescence can be fine-tuned by adjusting V_{ac} in the 10−80 V range. Visible light microscopy analysis shows that different grains reveal two or three different colors due to the polycrystalline nature of Zr, and the resultant coloration is the sum of these contributions. Reflectance spectroscopy spectra show maxima that can be related to the coloration displayed by various grains. Surface morphology and roughness in the micrometer and nanometer ranges are examined using stylus surface profilometry and atomic force microscopy. The formation of colored passive layers on polished Zr makes them smoother but their formation on etched Zr decreases the roughness in the case of low V_{ac} and increases in the case of high V_{ac}. Focused ion beam and scanning electron microscopy are used to determine the thickness (d) of the colored passive layer on etched Zr. It is found that d is in the 51−264 nm range and increases linearly with V_{ac}. Scanning transmission electron microscopy and electron back scattered diffraction measurements demonstrate that the colored passive layers are uniform and crystalline in nature. Corrosion behavior of the colored passive layers in 1 wt % aqueous NaCl solution is examined using inductively coupled plasma-mass spectrometry. The results indicate that the polished samples hardly undergo any corrosion and the amount of dissolved Zr does not exceed 12 ppb even after exposure for 56 days. On the other hand, the corrosion of the etched samples is ∼3 orders of magnitude greater than that of the polished ones, and the amount of dissolved Zr approaches 970 ppb after exposure for 56 days. Corrosion behavior of etched and colored passive layers on Zr in 1 wt % aqueous NaCl solution is also analyzed by recording potentiodynamic polarization curves in the −1.0 to 3.0 V vs RHE range at a scan rate of s = 1 mV s^{-1} and at T = 298 K. They have similar shapes but the formation of colored passive layers decreases the current density (j) at any given potential (E), and the thicker the passive layer the greater the reduction in j. The development of colored passive layers on etched Zr increases the corrosion potential (E_{corr}) and decreases the corrosion current density (j_{corr}).

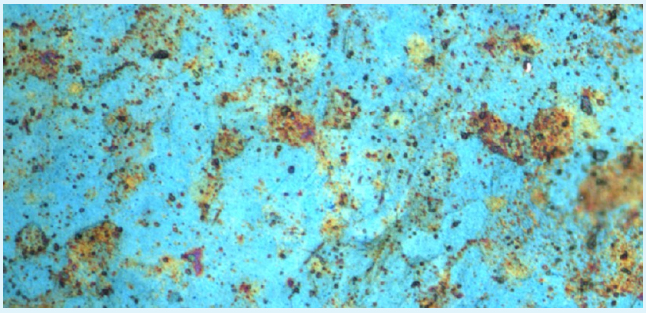

KEYWORDS: *zirconium, colored passive layers, ac polarization, morphology, corrosion, electrochemical characteristics*

INTRODUCTION

Zirconium (Zr) is a valve metal that similarly to titanium (Ti) finds usage in the aerospace and nuclear industries. The applicability of Zr in these highly demanding industries is possible due to its unique chemical and physical properties. Specifically, Zr has low density, high melting and boiling points, low heat transfer coefficient, high fire resistance, excellent mechanical properties (strength, ductility, and low thermal expansion coefficient), good performance at low and high temperatures, excellent resistance to abrasion, and resistance to various forms of corrosion.[1−5,6−8] Zirconium possesses several similar properties to Ti, but its melting and boiling points are significantly higher, thus making it a more suitable material when high-temperature applications are considered.[9] Upon solidification, Zr generates small grains and its surface appears smoother and shinier than that of Ti.[10] The successful application of Zr often depends on the presence of a surface passive layer that offers protective properties.[11] Passive layers on Zr often reveal coloration that originates from iridescence (constructive thin layer interference);[12−14] the coloration of passive layers is related to their thickness. Passive layers on Zr or Ti can be prepared through thermal oxidation at elevated temperatures or through electrochemical passivation in aqueous electrolyte solutions.[15−17] Thermal formation of passive layers is not an ideal technique as it is energy consuming because it requires the application of an elevated temperature (T = 800−

Received: July 19, 2012
Accepted: October 22, 2012
Published: October 22, 2012

   dx.doi.org/10.1021/am301389u | *ACS Appl. Mater. Interfaces* 2012, 4, 6487−6498

2000 °C) over a long time period (hours to days). Thermal passivation is known to produce layers the coloration of which ranges from blue to brown. Thermally prepared colored passive layers on Zr develop cracks (they have a "dry-mud" appearance) because the thermal expansion coefficients of the metal and the passive layers have different values. In regards to electrochemical treatment of Zr, both direct current (dc) and alternating current (ac) can be applied to form colored passive layers at an ambient temperature. The unique methodology developed in our laboratory employs ac polarization of Ti and Zr and suitable aqueous electrolyte solutions.[1,18] By adjusting the ac voltage (V_{ac}) and the passivation time, we can fine-tune the passive layer's thickness and, therefore, its coloration.[19] Interestingly, the application of ac voltage for short periods of time, typically 5−30 s, allows us to prepare a broad range of brightly colored layers. Preliminary X-ray photoelectron spectroscopy (XPS) measurements demonstrated that the chemical composition of passive layers on Zr formed by the ac polarization in aqueous Na_2SO_4 solution is ZrO_2.[20,21] Because the electrochemical passivation is carried out at room temperature, such formed protective layers do not develop fractures or other surface defects. The ability of Zr to develop stable passive layers which also reveal coloration opens up a wide range of potential applications in which both characteristics are required.

In this contribution, we discuss in detail the electrochemical method of forming colored passive layers on Zr and examine how the coloration depends on the sample pretreatment. We report on the optical properties, surface morphology, and thickness of the colored passive layers. We examine the stability of the colored passive layers under corrosion-promoting conditions.

EXPERIMENTAL SECTION

Zirconium Electrodes, Electrolyte, and Cell. Circular, square, and wire zirconium samples were used in the course of research. The circular and square electrodes were used in morphology and coloration characterization, and the wire-shaped electrodes were used in electrochemical studies. The circular and square Zr electrodes were made of Zr sheet (Johnson-Matthey, 99.6 wt % containing 0.12% Fe, 0.08% Si, 0.05% C, 0.10% O, and 0.04% N) and were either 7 or 10 mm in diameter and 1.00 ± 0.01 mm (0.039 in) in thickness. They were spot-welded to a Zr wire (Aldrich, 99.7 wt %) for electrical contact. The circular and square electrodes were degreased in acetone under reflux in order to remove any organic impurities. Subsequently, they were etched for 7−12 min in an etching solution made from 30 cm^3 of concentrated HF and 50 cm^3 of concentrated HNO_3 diluted to 1000 cm^3 with deionized water (Millipore 18.2 MΩ cm); afterward, they were thoroughly rinsed with deionized water. The wire-shaped electrodes were made of Zr wire (Aldrich, 99.7 wt % and 0.81 ± 0.02 mm in diameter). They were connected to a copper wire in an insulating sleeve through an electric connector; the Zr wire-copper wire connection was sealed with epoxy resin (Struers), and only the Zr wire was in contact with electrolyte. Upon the resin hardening, the Zr wire was cut to a length of 1.00 ± 0.05 cm, and the incision was polished with sandpaper using a mechanical polisher (Struers) to reach a flat end. The wire-shaped Zr electrodes were subsequently degreased in acetone and rinsed with deionized water. Then, they were treated in the etching solution described above, rinsed with deionized water, and sonicated in an ultrasonic bath (Branson) for 1 min. Both the circular and wire-shaped Zr electrodes were immersed in a single compartment electrochemical cell where the electrochemical coloration was carried out by applying an ac voltage. The counter electrode was made of Pt foil spot-welded to a Pt wire (Johnson-Matthey, 99.9 wt %); its real surface area was at least 10 times greater than that of the Zr electrode. The distance between the Zr and Pt electrodes was maintained at ∼5 cm; this separation was sufficient to allow for effective circulation of the electrolyte between the electrodes and for removal of the gases generated during the ac polarization. In general, the preparation procedure applied in the course of research guaranteed good reproducibility of the experimental results. In order to ensure uniform coloration of the Zr electrode, the ac polarization was performed at well-controlled temperature (T) conditions, here T = 298 K, achieved by placing the cell in a water bath and by passing a stream of N_2(g) through the cell.

Polarization curves for Zr and colored passive layers on Zr were recorded in 1 wt % aqueous NaCl solution in a standard, two-compartment electrochemical cell. This solution of NaCl was selected for the following reasons: (i) to mimic a typical saline environment; (ii) to simulate a corrosive medium in which metallic corrosion studies are typically performed; and (iii) to simulate a physiological body fluid that normally contains NaCl.[22] A stream of Ar(g) (99.99 wt %) was passed through the electrolyte to maintain a neutral environment and to expel any gases generated during electrochemical characterization. A Pt/Pt black reversible hydrogen electrode (RHE) was used as a reference electrode in the electrochemical characterization (polarization curves).

Morphology Characterization. The uniformity of surface coloration and morphology of the colored Zr passive layers was examined by means of visible light microscopy (VLM) using a low-resolution Seiwa Optical SDMTR microscope and a high-resolution Zeiss AXIO Imager M2MAT visible light microscope. The VLM studies were followed by atomic force microscopy (AFM) surface topography experiments conducted using a Veeco Instruments MultiMode 8 scanning probe microscope. For tapping mode measurements, a Veeco phosphorus (n) doped silicon tip (model RTESP) was employed with a spring constant in the 20−80 N m^{-1} range. Resonance frequency was in the 248−357 kHz range, and the nominal tip radius of curvature was in the 5−10 nm range. For contact mode experiments, a Veeco silicon tip on a nitride lever (model SNL-10) was employed with a spring constant of 0.12 or 0.58 N m^{-1} depending on which side of the tip was employed. The tip radius was in the 14−75 nm range. Scan sizes varied from 1 to 15 μm, with the 15 μm topography maps being shown in the Results and Discussion section and employed for surface roughness evaluation. Scan rate, integral gain, and proportional gain were altered in order to optimize the parameters and to provide a quality image in each scan. Surface profiling and roughness measurements were also carried out using a stylus profiler (Veeco Dektak 8 Stylus Profiler).

UV−Visible-NIR Reflectance Spectroscopy. Reflectance spectroscopy measurements were conducted using a UV−vis-NIR light source (DH-2000-BAL) that was connected to a high-resolution spectrometer (HR-4000, Ocean Optics) using optical fibers. The spectrometer was capable of detecting in the 200−1100 nm wavelength (λ) range. The light source had a range of 215−400 nm (deuterium light source) and 360−2000 nm (tungsten-halogen light source). The use of this combined

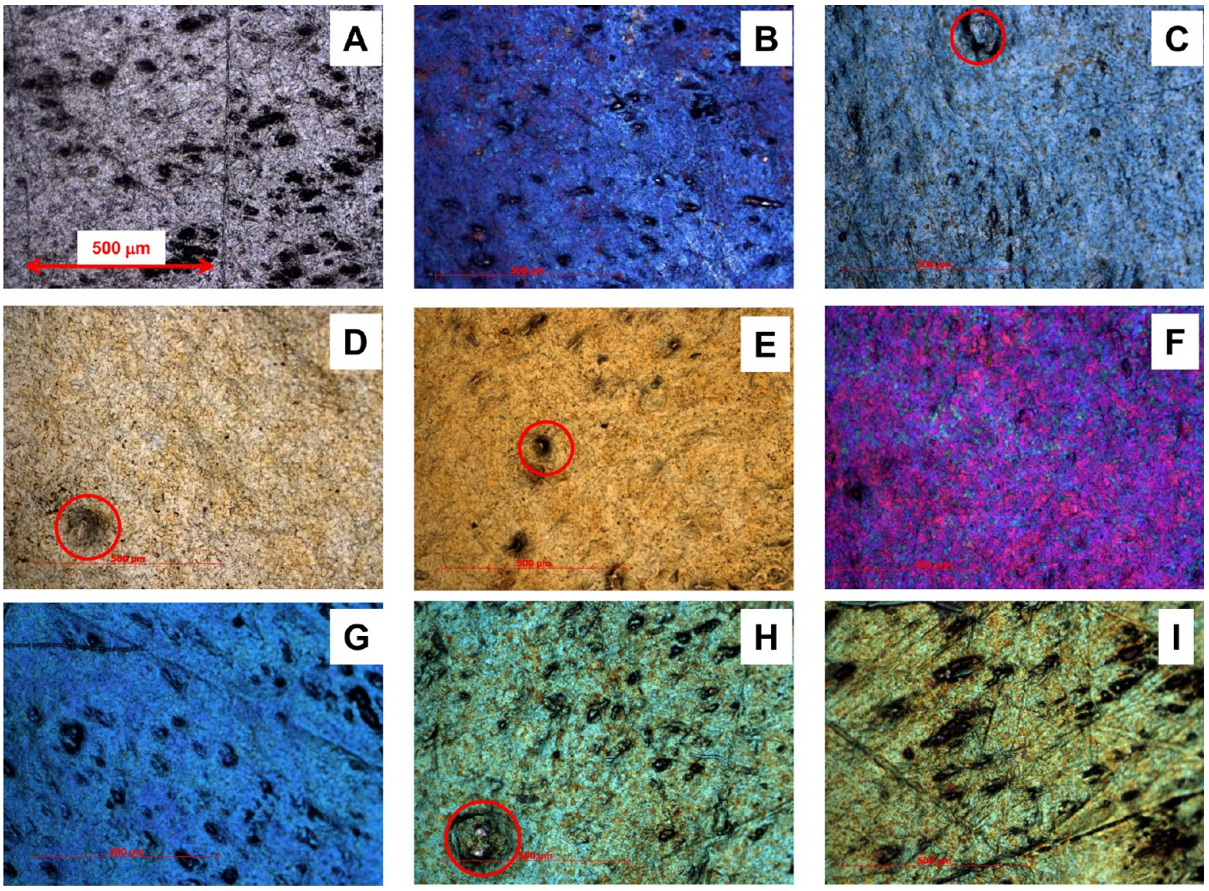

Figure 1. Visible light microscopy images of the colored passive layers on etched Zr formed in 10 wt % aqueous Na_2SO_4 solution by applying an ac voltage for 10 s at T = 298 K. The image A presents nonpassivated Zr; the images B through I refer to the colored passive layers formed at V_{ac} = 10, 20, ..., 80 V. The magnification is the same in each case, and the scale bar refers to 500 μm. Red circles mark pore-like surface defects.

deuterium and tungsten-halogen light source allows for elimination of saturation and increase of the signal-to-noise ratio. A mirror (STAN-SSH High-reflectivity Specular Reflectance Standard) was employed for the collection of a background spectrum before any measurements were taken. The data were acquired and processed using the Spectra Suite (Ocean Optics Inc.) software. During the collection of the data, an integration time of 200 ms was used, along with an average of 50 acquisitions and a boxcar average of 10 data points.

SEM-FIB/TEM/EBSD. A Zeiss AURIGA Cross Beam instrument was employed to conduct scanning electron microscopy (SEM), focused ion beam (FIB), and transmission electron microscopy (TEM) analyses. Coupled FIB-SEM measurements allowed determination of the thickness of the colored passive layers on Zr. Transmission electron microscopy and electron backscatter diffraction (EBSD) measurements were carried out to examine whether the passive layers were crystalline or amorphous in nature.

ICP-MS. Inductively coupled plasma-mass spectrometry (ICP-MS) experiments were performed using a Varian 820-MS instrument, with a Dionex 600/BioLC liquid chromatography system equipped with a GS50 gradient pump, a Rheodyne 9750E injector, and a 50 μL sample loop, employed for flow injection. The matrix was a 1 wt % aqueous NaCl solution. The specimens were all placed in test tubes containing 25.0 mL of the 1 wt % aqueous NaCl solution and were sealed with silicone stoppers. The pump was stabilized by pumping a carrier solution (deionized water, Millipore) for 60 min. The torch was aligned using a tuning solution containing 5 $\mu g\ L^{-1}$ of Be, Mg, Co, In, Ce, Pb, and Ba in 1 wt % HNO_3 in deionized water solution prepared by dilution from a 10 $\mu g\ L^{-1}$ Varian tuning solution (Spectropure, St. Louis, MO). For signal optimization, the nebulizer, torch, sampler, and skimmer cones were cleaned and a full optimization procedure was performed, including plasma alignment, mass calibration, mass resolution and trim, detector setup, and ion optic settings. The samples were run in time-resolved mode (peak hopping), with a sample uptake rate of 1 mL min^{-1}. A five point external calibration was employed (linear regression through the origin): blank, 1, 10, 50, and 100 ppb. The detection limit was 0.1 $\mu g\ L^{-1}$ for the Zr solutions. The ICP-MS standards (SCP Science, Champlain, NY) were used to prepare calibration standards in 1 wt % aqueous NaCl solution, which was also used as a blank. The error value on the slopes of the calibration curves is 23 490 $\pm$ 680 (2.9%) for Zr.

Electrochemical Instrumentation. The colored passive layers on Zr were prepared using a variable ac power supply at a frequency of 60 Hz (Vector-Vid, Instrument Division, WP32), and the applied V_{ac} was monitored by means of a multimeter (Fluke 45). Electrochemical characterization was performed using an Autolab model PGSTAT 302N potentiostat. The software package employed was the NOVA 1.6 electrochemical and corrosion software; it was used to control experimental parameters and to acquire data. Polarization curves of the wire-shaped Zr electrodes in 1 wt % aqueous NaCl solution were obtained in the −1.0 to +3.0 V versus RHE potential range. In

these measurements, the counter electrode was made of a platinum mesh, and its surface area was over 10 times that of the Zr working electrodes. All current densities (j) are reported with respect to the geometric surface area of the Zr electrodes.

RESULTS AND DISCUSSION

Coloration and Appearance of Passive Layers on Zr. Polycrystalline Zr were colored by the application of controlled V_{ac}. The as-received Zr specimens (wires, sheets), which were manufactured using pulling and rolling methods, did not reveal any crystallites or grains by visual inspection because the topmost layer was mechanically disordered. However, after cleaning and etching, they revealed a well-defined grain structure with clearly visible individual crystallites and boundaries in between. It is important to add that the individual grains observed by VLM (see below) correspond to crystals because pure metals do not develop amorphous structures. Because every grain in the polycrystalline Zr sample behaves like a single crystal, it became necessary to examine whether (a) different crystallites possessed the same coloration; (b) the surface roughness underwent any changes upon the colored passive layer formation, and if so how it depended on V_{ac}; and (c) the colored passive films revealed cracks or other surface defects.

In order to examine the influence of surface pretreatment on the ability of Zr to develop colored passive layers by applying ac polarization and on the coloration uniformity, we polarized both mechanically polished and chemically etched samples. Although the results of surface topography measurements will be discussed in a later section, at this stage of the discussion we wish to report that the average roughness value determined using surface profilometry ($R_{a,profile}$) of mechanically polished Zr was 0.329 ± 0.017 μm and that of chemically etched Zr was 0.505 ± 0.023 μm. Visual inspection and low-magnification VLM analysis indicated that the application of a specific V_{ac} produced uniformly colored passive layers but the coloration was different between the mechanically polished and chemically etched samples. These results indicate that the sample pretreatment has an impact on the formation of colored passive layers and affects their thickness. The mechanically polished samples reveal scratches that remain pronounced even after the coloration. The chemically etched samples produce a mosaic-like (granite-like) appearance due to different grains having different colors. Chemical etching exposes the well-defined grain (crystallite) structure of Zr that develops during its solidification, while mechanical polishing disorders the topmost layer of Zr making crystallites difficult to perceive and introduces mechanical strain.

Figure 1 presents VLM images obtained using Zeiss AXIO Imager M2MAT of chemically etched Zr (image A; it serves as a reference) and chemically etched and colored Zr samples (images B through I). The images clearly demonstrate that not all grains have the same coloration but in each case a predominant color emerges. The untreated Zr (image A) is gray but has slight violet coloration. The passive layer formed at V_{ac} = 10 V (image B) has an overall dark blue coloration with sparsely distributed reddish brown grains. The passive layer formed at V_{ac} = 20 V (image C) has an overall light blue coloration with some yellowish grains. The passive layer formed at V_{ac} = 30 V (image D) has an overall yellow coloration with a slight green tint. The passive layer formed at V_{ac} = 40 V (image E) has an overall orange-golden coloration. The passive layers formed at V_{ac} = 50 V (image F) has an overall violet coloration with some grains being red, blue, and green. The passive layer formed at V_{ac} = 60 V (image G) has an overall blue coloration with a green tint, which originates from some green grains. The passive layer formed at V_{ac} = 70 V (image H) has an overall teal coloration (slightly turquoise) with some orange grains. Finally, the passive layer formed at V_{ac} = 80 V (image I) has an overall light green coloration that seems to originate from teal and orange grains that have similar distributions. It is interesting to observe that although three different samples have bluish coloration, the actual colors are distinctly different. The analysis of VLM images also reveals the presence of pore-like surface defects (red circles in Figure 1) the size and distribution of which increase as V_{ac} is raised (see AFM results in a later section). These pore-like defects have been observed previously in passive layers on Ti and were also correlated with V_{ac}.[23,24] We do not report results for V_{ac} > 80 V because the application of such high V_{ac} leads to electrical breakdown of the passive layers, which is accompanied by visible sparking and audible cracking. The results of VLM measurements may be summarized as follows: (i) the surface coloration is predominantly uniform; (ii) when different grains have the same overall coloration, they are covered with passive layers having the same thickness; (iii) certain grains show slightly different coloration than that expected for a particular V_{ac} value and in this case the thickness of the passive layers is not the same on different grains; (iv) the colored passive layers have pore-like defects; and (v) the colored passive layers are free of micrometer-sized cracks. The observation that different grains within a polycrystalline Zr sample have different colors indicates that the surface coloration depends on their crystallographic orientation (see the section Ion Beam and Electron Microscopy Characterization).

Surface Morphology of Colored Passive Layers on Zr. Surface morphology and roughness of the colored passive layers on Zr were analyzed using stylus surface profilometry and atomic force microscopy. The surface profilometry and atomic force microscopy examine the surface roughness and topographical characteristics in the micrometer and nanometer ranges, respectively. Surface profilometry was employed to determine the average surface roughness (R_a) of the colored passive layers by recording four topography maps (2.5 mm × 2.5 mm) per sample. Table 1 summarizes the average surface roughness values determined using profilometry ($R_{a,profile}$) for two sets of Zr samples, namely, the colored passive layers formed on mechanically polished and chemically etched

Table 1. Average Surface Roughness Determined through Profilometry Measurements ($R_{a,profile}$) of Untreated and Electrochemically Colored Zr in Relation to the Applied ac Voltage and Surface Pretreatment[a]

V_{ac} (V)	$R_{a,profile}$ (μm) for polished Zr	$R_{a,profile}$ (μm) for etched Zr
0	0.329 ± 0.017	0.505 ± 0.023
10	0.217 ± 0.022	0.462 ± 0.105
20	0.164 ± 0.021	0.458 ± 0.023
30	0.161 ± 0.020	0.506 ± 0.054
40	0.066 ± 0.013	0.406 ± 0.112
50	0.149 ± 0.010	0.414 ± 0.065
60	0.277 ± 0.023	0.580 ± 0.010
70	0.289 ± 0.007	0.696 ± 0.033
80	0.188 ± 0.091	0.727 ± 0.058

[a] V_{ac} = 0 V refers to nonpassivated Zr.

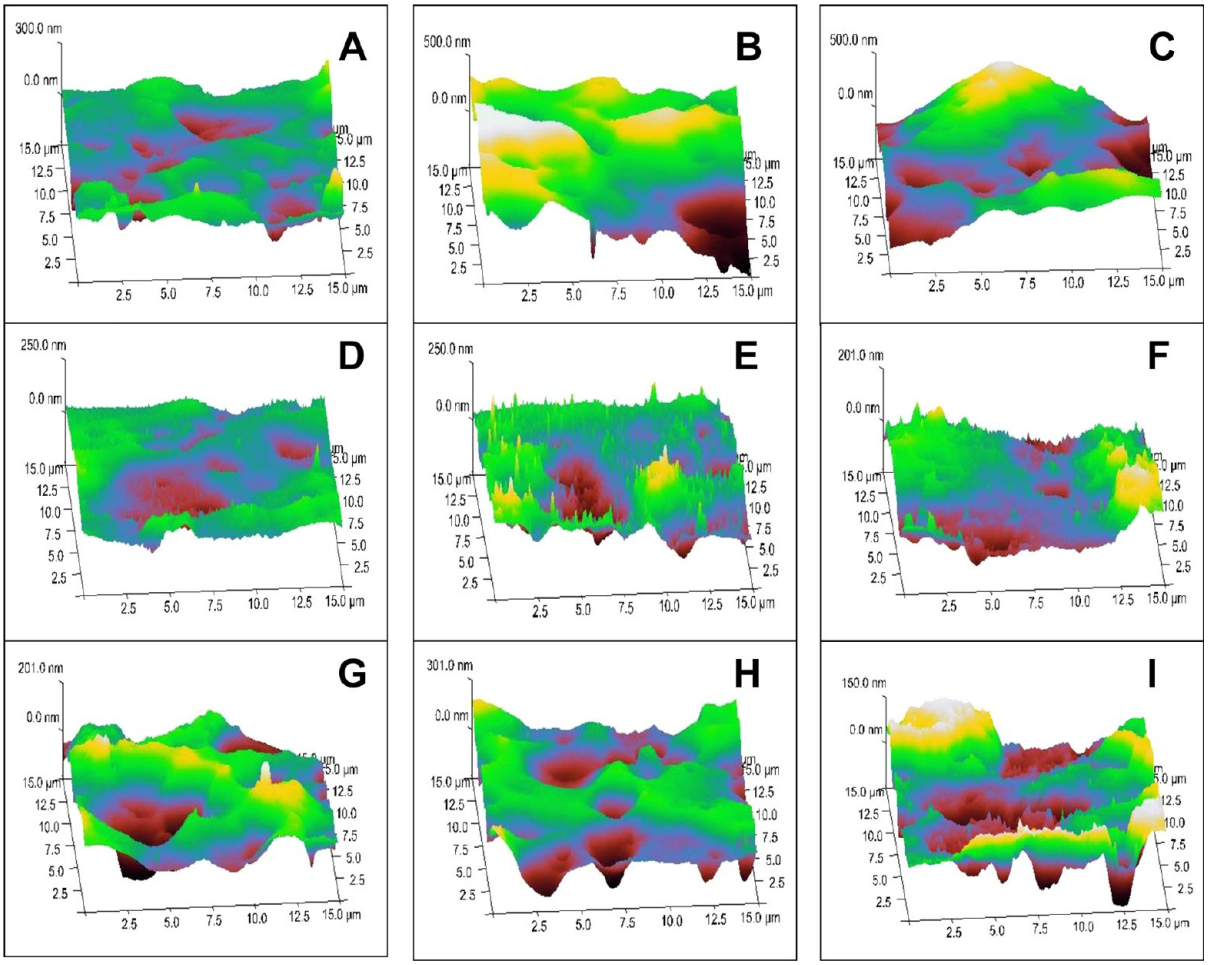

Figure 2. Atomic force microscopy topographical maps (sample area = 15 μm × 15 μm) for the colored passive layers formed on Zr. The image A refers to nonpassivated Zr; the images B through I refer to the colored passive layers formed at V_{ac} = 10, 20, ..., 80 V.

specimens. As expected, the $R_{a,profile}$ values demonstrate that the polished samples are less-rough than the etched ones. The formation of a colored passive layer through the application of $V_{ac} \leq 50$ V decreases $R_{a,profile}$ but the formation of a colored passive layer by the application of $V_{ac} \geq 60$ V increases $R_{a,profile}$. The former behavior can be related to a smoothing effect associated with a passive layer formation and the latter behavior can be associated with the development of surface pore-like defects. This roughness trend agrees with similar results obtained for the colored passive layers on Ti.[25] In Figure 2, we present AFM topographical maps (sample area = 15 μm × 15 μm) for chemically etched and electrochemically formed colored passive layers on Zr. Table 2 summarizes the $R_{a,AFM}$ values for the etched Zr samples. The results of AFM analysis lead to the following observations: (i) the colored passive layers reveal a similar morphology to that of nonpassivated Zr; (ii) the surface morphology of nonpassivated and passivated Zr resembles rolling hills and valleys (spikes at some hill-valley transitions are experimental artifacts); (iii) the average surface roughness determined using AFM measurements ($R_{a,AFM}$) for the etched Zr is ∼43 nm and increased by a factor of ∼2.5 as colored passive layers are formed at V_{ac} = 10 and 20 V; (iv) the values of $R_{a,AFM}$ for the colored passive layers formed at V_{ac} = 30, 40, and 50 V are very similar to that of nonpassivated Zr; (v) the values of $R_{a,AFM}$ for the colored passive layers formed at V_{ac} = 60, 70, and 80 V gradually increase by a factor of 1.25, 1.5, and 1.6, respectively, as compared to nonpassivated Zr; and (vi) there are no new features. We employed AFM to examine the dimensions of the valleys and determined that their size is in the 1.7−8.0 μm range and their depth varies from 22 to 43 nm. The trend identified on the basis of AFM measurements agrees with that observed through surface profilometry experiments.[26,27] This trend is an increase in roughness as passive layer thickness increases, especially at higher applied voltages, where the initial $R_{a,AFM}$ for nonpassivated Zr was 43.3 ± 3.9 nm, and the $R_{a,AFM}$ value for Zr passivated at V_{ac} = 80 V was 67.4 ± 10.6 nm. Elsewhere,[19] it was explained that the electrochemi-

Table 2. Average Surface Roughness Determined through AFM Measurements ($R_{a,AFM}$) of Chemically Etched, Electrochemically Colored Zr[a]

V_{ac} (V)	$R_{a,AFM}$ (nm)
0	43.3 ± 3.9
10	111.3 ± 8.6
20	100.4 ± 8.0
30	39.2 ± 6.8
40	47.2 ± 5.9
50	47.9 ± 6.6
60	53.9 ± 3.7
70	67.4 ± 10.6
80	70.4 ± 5.8

[a] V_{ac} = 0 V refers to nonpassivated Zr.

dx.doi.org/10.1021/am301389u | ACS Appl. Mater. Interfaces 2012, 4, 6487−6498

cally formed colored passive layers on Ti and Zr not only offer unique decorative properties[27−29] but might also find application as biomaterials.[30] Specifically, rougher surfaces enable osseointegration of implants and offer a porous structure that facilitates cell adhesion. Because the electrochemically formed colored passive layers on Zr are rough, they might possibly find application as medical and dental implants.

UV−Visible-NIR Reflectance Spectroscopy. Reflectance spectroscopy measurements were conducted using an ultraviolet−visible-near-infrared (UV−vis-NIR) light source which was connected to a high-resolution spectrometer using fiber optics. These experiments were carried out with the objective of identifying wavelength regions with strong intensity and comparing them to the coloration observed by VLM (Figure 1). We studied two sets of samples, namely, polished and colored Zr, and etched and colored Zr. The wavelength range covered in these measurements was λ = 200−1100 nm. The results are presented as the reflectance (R) versus λ; the reflectance is defined as $R = I_{refl}/I_{incid}$, where I_{refl} and I_{incid} are the reflected and incident spectral intensities. The values of R are in the 0−1 range, with R = 1 referring to all light being reflected. Although the visible spectrum covering the λ = 400−780 nm range is of the greatest importance in the analysis of coloration, we also examined the UV and NIR ranges in order to determine whether there were any other noticeable spectral features. Figure 3 presents reflectance spectra for the colored passive layers formed on both polished (left-hand side) and etched (right-hand side) Zr specimens. We observe that the reflectance spectra obtained using both polished and etched Zr samples have similar intensities. This observation is not surprising because Zr upon solidification develops small grains and its chemical etching yields a mirror-like surface. Thus, both polished and etched Zr samples were very smooth and reflective. The spectra for V_{ac} = 0 V refer to nonpassivated Zr and serve as references; they display a similar trend in the value of R with increasing λ up to 780 nm. This trend is due to the refractive index being dependent on wavelength; this is a common behavior observed with high refractive index substances such as metals. These spectra also display features in the 420−500 nm region, indicating that both spectra have contributions in the blue and violet regions of visible light. This observation is corroborated by VLM results (image A in Figure 1) which show that untreated Zr has light purple appearance. In the case of V_{ac} = 10 V, the reflectance spectra have similar shapes but in the case of the etched sample the intensity in the violet and blue regions is high giving rise to dark-blue coloration (image B in Figure 1). In the case of V_{ac} = 20 V, the reflectance spectra have different shapes. The spectrum for the polished sample shows a broad region of high intensity in the λ = 400−600 nm range, which gives the sample a dark bluish-purple appearance. The etched sample shows a broad region of high intensity in the λ = 450−650 nm range, which gives the sample a blue color with a slightly yellow tint (image C in Figure 1). In the case of V_{ac} = 30 V, the two reflectance spectra have different shapes. The polished sample shows high reflectance predominantly in the blue, violet, and green regions, which give rise to a light-blue appearance. The etched sample has high reflectance in the green, yellow, and orange regions, thus producing a yellowish beige coloration (image D in Figure 1). In the case of V_{ac} = 40 V, the two reflectance spectra are different. The polished sample has high reflectance in the yellow and orange regions, with contributions from green and blue lights, thus giving the sample yellowish green coloration.

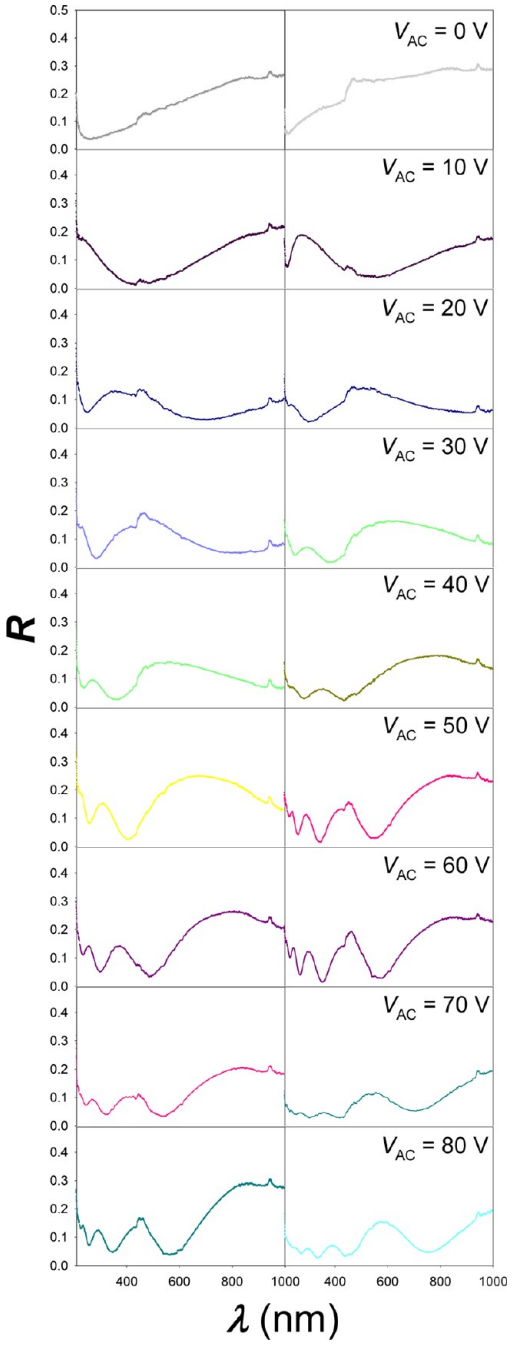

Figure 3. Reflectance spectra (R vs λ) in the λ = 200−1000 nm range for the colored passive layers formed on mechanically polished (left-hand side) and chemically etched (right-hand side) Zr. The line colors are selected to present as closely as possible the actual coloration observed visually.

In the case of the etched sample, the reflectance spectrum shows high intensity in the yellow, orange, and red regions, thus producing an overall yellowish orange (golden) coloration (image E in Figure 1). In the case of V_{ac} = 50 V, the reflectance spectra are significantly different. The polished sample has high intensity in the green, yellow, orange, and red regions, which produce yellow-orange coloration. The etched sample produces a spectrum with high intensities in the violet, blue, and red regions, which together generate overall bright magenta coloration (image F in Figure 1). In the case of V_{ac} = 60 V, the reflectance spectra have similar shapes. The polished sample

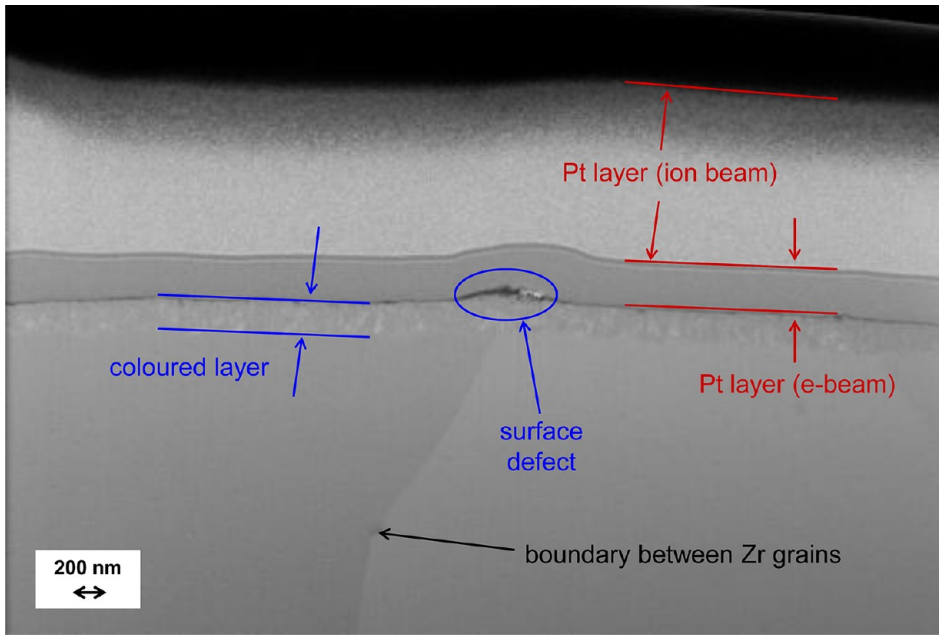

Figure 4. Scanning electron microscopy cross section image generated using secondary electrons of the colored layer on Zr formed by applying V_{ac} = 80 V. The cross section was prepared by Ga-ion beam machining.

has high intensity in the violet, yellow, orange, and red regions, thus producing dark violet coloration. The etched sample has high intensity in the violet, blue, and red regions, which generate a purplish dark blue appearance (image G in Figure 1). In the case of V_{ac} = 70 V, the spectra are different. The polished sample shows high intensity in the violet, blue, orange, and red regions, which create an overall magenta coloration but less bright than the one obtained for the etched sample at V_{ac} = 50 V. The etched sample shows high intensity in the blue, green, yellow, and orange regions, which produce an overall teal coloration (image H in Figure 1). Finally, in the case of V_{ac} = 80 V, the reflectance spectra are different. The polished sample has high intensity in the blue and green regions, thus producing a greenish-blue coloration. The etched sample shows high intensity in the blue, green, yellow, and orange regions, thus generating an overall bluish-teal coloration (image I in Figure 1). The bluish tint originates from the combination of teal and orange-yellow grains observed in image I in Figure 1.

It is interesting to observe that the application of a given V_{ac} generates very different colorations and textures in the case of polished and etched Zr samples. This difference is attributed to different thicknesses of the passive layers formed on polished and etched samples. The distinct textures of the colored passive layers obtained in the case of the polished and etched samples can be attributed to structural differences introduced by the mechanical polishing and chemical etching. We observe that the application of a progressively higher V_{ac} results in a gradual shift of the spectral features toward longer wavelengths (a red shift). We also notice that as a spectral feature shifts toward the infrared region, a new feature appears within the UV range. This observation indicates that as the applied V_{ac} increases and the thickness of passive layer increases, different wavelengths contribute to the constructive and destructive interference.[27]

Ion Beam and Electron Microscopy Characterization. Focused ion beam, scanning electron microscopy, transmission electron microscopy, and electron backscatter diffraction measurements were performed with the following objectives: (i) to determine the thickness (d) of the colored passive layers on Zr; (ii) to examine the thickness uniformity; and (iii) to evaluate crystalline properties of the colored passive layers. In order to carry out the thickness analysis, the samples were initially coated with a platinum (Pt) layer using first electron-beam deposition and then ion-beam deposition. The Pt layer offered protection from gallium-ion implantation and other artifacts during ion-beam machining. In addition, the Pt protective layer was used to attach samples to a Pt grid employed in TEM measurements using an ion beam. Figure 4 shows an SEM image generated using secondary electrons of a typical cross section prepared by Ga-ion beam machining; in this case, the colored passive layer was prepared on chemically etched Zr and the coloration voltage was V_{ac} = 80 V. It reveals the colored passive layer, the two Pt protective layers, Zr grains and a grain boundary, and a surface defect. The SEM image was used to evaluate the thickness of the colored passive layer in several sections and to determine an average thickness. Similar measurements were performed on all the colored passive layers formed at $10 \leq V_{ac} \leq 80$ V. Figure 5 presents a graph of d as a function of V_{ac} for the colored passive layers prepared on etched Zr. They demonstrate that as the value of V_{ac} required to form them increases (with other parameters being constant), their thicknesses also increase. As expected, the thinnest layer is obtained in the case of V_{ac} = 10 V and d = 51 ± 4 nm, and the thickest layer is obtained in the case of V_{ac} = 80 V and d = 264 ± 15 nm. We extrapolated the d vs V_{ac} plot to V_{ac} = 0 V in order to determine the thickness of a native passive layer that develops on Zr during its handling in and exposure to air; such a determined thickness was found to be 19 ± 2 nm. This is a reasonable value because metallic Zr prepared by chemical etching is very reactive; upon contact with air, its appearance changes from sparkling metallic to dull metallic within several minutes. The slope of the d vs V_{ac} plot equals 3.06 nm V^{-1}, indicating that an increase of the applied V_{ac} by 1 V while maintaining other parameters constant increases the thickness of the colored passive layer by ~3 nm. This is a very important observation because it demonstrates that the thickness of the

dx.doi.org/10.1021/am301389u | ACS Appl. Mater. Interfaces 2012, 4, 6487−6498

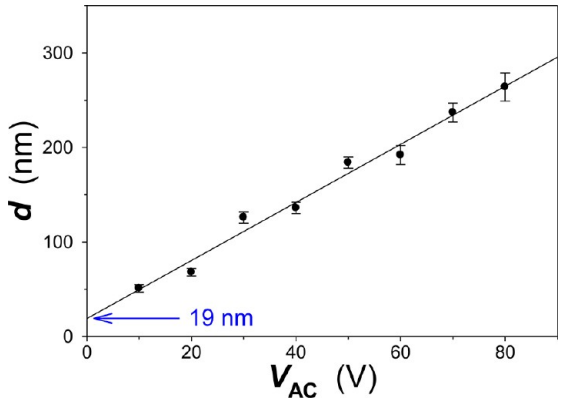

Figure 5. Graph of the thickness (d) of the colored passive layers on etched Zr as a function of the ac voltage (V_{ac}) required to form them. Extrapolation of the d vs V_{ac} plot to V_{ac} = 0 V results in the determination of the thickness of the native oxide layer covering etched Zr.

colored passive layers can be controlled with the precision of several nanometers simply through fine control of V_{ac}.

In a separate series of measurements, we used scanning transmission electron microscopy (STEM) and electron backscatter diffraction (EBSD) to examine whether the colored passive layers were crystalline or amorphous in nature. In Figure 6, we present an STEM dark field image for the passive layer formed at V_{ac} = 80 V that reveals an ordered structure. The image suggests that the passive layer might be crystalline in nature. It also shows long leaf-shaped features that originate from mechanical stress in the underlying Zr substrate. Because the manufacture of Zr sheets and plates involves rolling, there is a significant mechanical strain within the Zr metal sheet. The hypothesis that the colored passive layers could be crystalline was examined by recording EBSD patterns and identifying Kikuchi patterns that are observed only in the case of crystalline samples. Figure 7 presents EBSD patterns for the nonpassivated Zr substrate (image A) and the colored passive layer formed at V_{ac} = 80 V (image B). The assignment of the Kikuchi lines for Zr and the colored passive layer is presented in images C and D of Figure 7, respectively. The presence of well-defined Kikuchi lines proves that the electrochemically colored passive layers are crystalline in nature. The EBSD imaging was limited to the colored passive layer formed at V_{ac} = 80 V because an analysis of the thickest layer offered the best quality of imaging. However, the observation that the colored passive layers are crystalline in nature most likely applies to all colored passive layers formed on etched Zr because the application of a specific V_{ac} value modifies the passive layer's thickness without introducing any other major structural changes.

ICP-MS Analysis. Inductively coupled plasma-mass spectrometry studies were performed on two sets of Zr samples, polished and etched, that were electrochemically passivated by applying $10 \leq V_{ac} \leq 80$ V; the nonpassivated Zr samples (V_{ac} = 0 V) serve as references. The Zr samples were placed in 25 mL of 1 wt % aqueous NaCl solution for various exposure times (t_{exp}) up to 8 weeks. An aliquot of the aqueous NaCl solution was collected after 24 h (1 day), 168 h (7 days), 336 h (14 days), 672 h (28 days), and 1344 h (56 days), respectively, and the amount of Zr in the solution was analyzed by ICP-MS. Figure 8 presents the amount of dissolved Zr expressed as concentration (c) in ppb as a function of the exposure time (t_{exp}) and V_{ac} for the polished (graph A) and etched (graph B) Zr samples. In general the longer t_{exp}, the greater the amount of dissolved Zr but the data obtained for the polished and etched samples are dramatically different. In the case of polished samples (graph A in Figure 8), the amount of Zr in the 1 wt % aqueous NaCl solution never exceeds 12 ppb. In addition, the development of colored passive layers on Zr does not impact the amount of dissolved Zr that is practically the same within ±0.5 ppb. This observation is not surprising because Zr is known to resist various acidic, alkaline, and saline aqueous solutions, and the 1 wt % aqueous NaCl solution employed in the course of research is a mild medium. In the case of etched

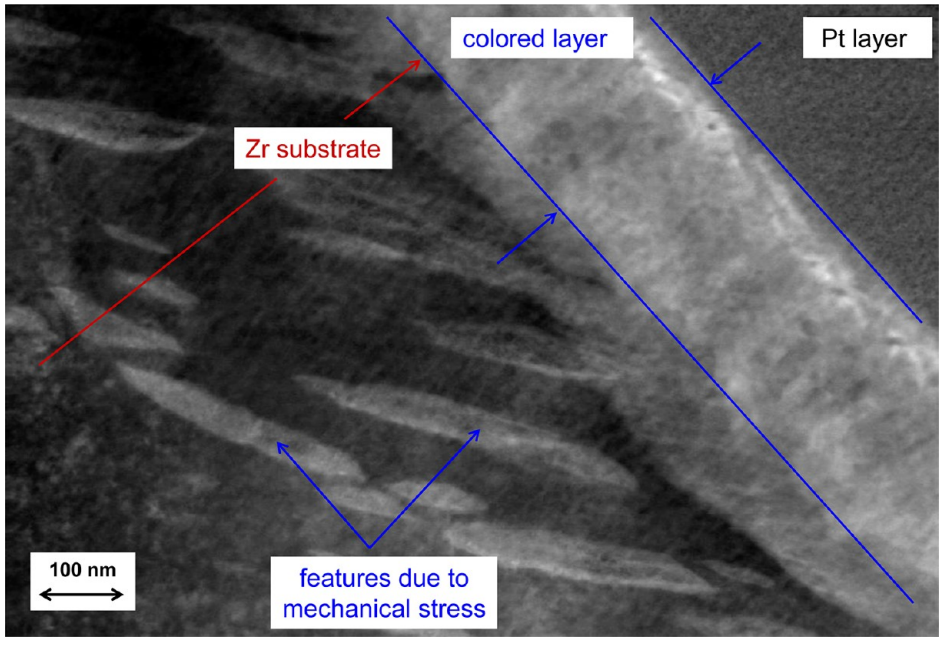

Figure 6. Scanning transmission electron microscopy image for a cross section of the colored layer formed at V_{ac} = 80 V showing the passive layer and the substrate. The scale bar refers to 100 nm.

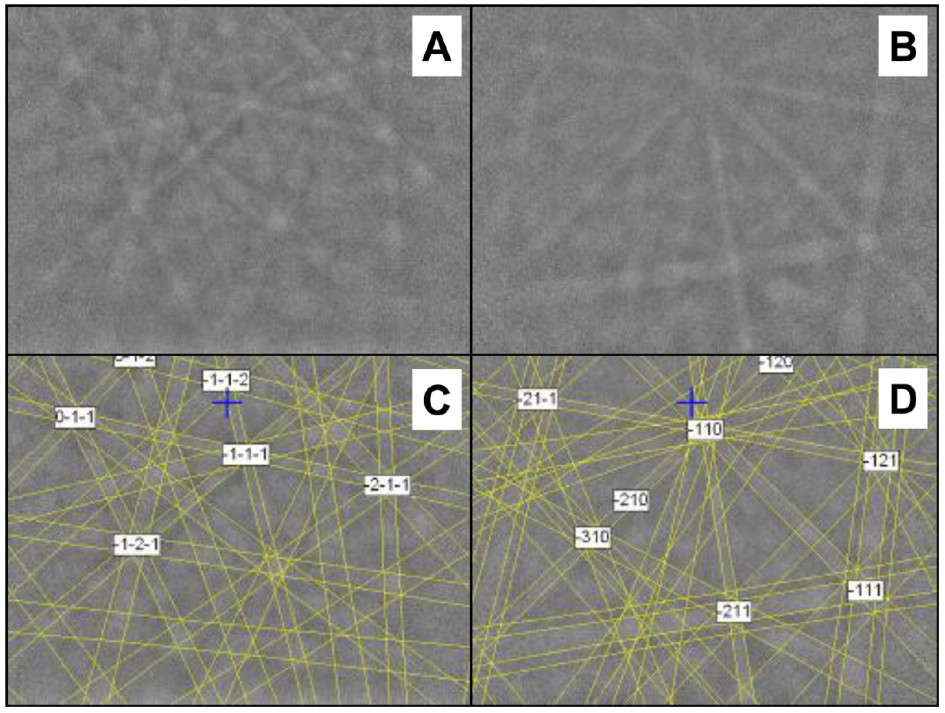

Figure 7. Electron backscatter diffraction patterns for the nonpassivated Zr substrate (image A) and the colored passive layer formed at V_{ac} = 80 V (image B). The assignment of the Kikuchi lines is presented in the images C and D, respectively.

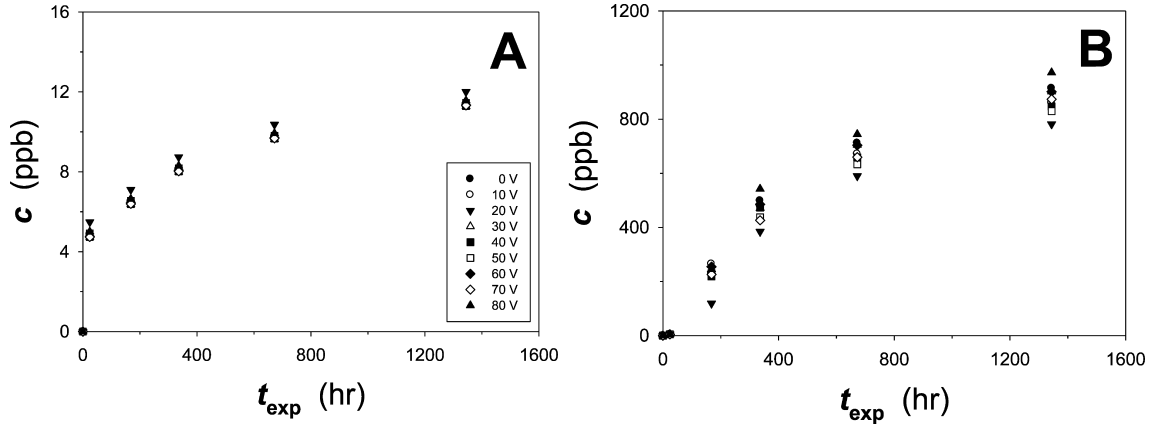

Figure 8. Amount of dissolved Zr upon exposure to 1 wt. % aqueous NaCl solution expressed as concentration (c) in ppb. It is presented as a function of the exposure time (t_{exp}) and V_{ac} for the polished (graph A) and etched (graph B) Zr samples.

samples (graph B in Figure 8), the amount of dissolved Zr in the 1 wt % aqueous NaCl solution is almost 3 orders of magnitude higher than in the case of polished samples and approaches 970 ppb for t_{exp} = 1344 h. The development of colored passive layers impacts the amount of dissolved Zr but the respective differences for a given V_{ac} never exceed 20%. These unexpected results demonstrate that the pretreatment applied to Zr prior to the formation of colored passive layers by ac polarization has a profound impact on its dissolution in an aqueous NaCl solution. These results agree with those obtained by Mogoda[31] and others,[32,33] who found that chemically etched Zr experienced a greater dissolution rate than polished Zr.

Polarization Curves. In order to advance our understanding of the corrosion behavior of Zr in 1 wt % aqueous NaCl solution, we recorded potentiodynamic polarization curves for colored passive layers on Zr as well as for a nonpassivated etched Zr sample (V_{ac} = 0 V); the latter was used in a comparative data analysis. We focused our analysis only on the etched Zr samples because the polished samples revealed very low dissolution rates as determined through ICP-MS measurements; thus, their corrosion rates were extremely low. Potentiodynamic polarization curves were recorded in the potential range from −1.0 to +3.0 V at a scan rate of s = 1 mV s^{-1} and at a temperature of T = 298 K (Figure 9). The graphs A−H present two polarization curves, one for etched and nonpassivated Zr (gray line) and the other for a colored passive layer formed at a given V_{ac} (black line). A simple qualitative analysis leads to the following observations: (i) all polarization curves have similar shapes with the exception of the curves for the colored passive layers formed at V_{ac} = 10 and 20 V that show an additional small feature at ~E = 0.4 V; (ii) the polarization curves do not show features characteristic of active-passive transition;[16] (iii) at any given E, the value of j for a colored passive layer is always smaller than that for non-

dx.doi.org/10.1021/am301389u | ACS Appl. Mater. Interfaces 2012, 4, 6487−6498

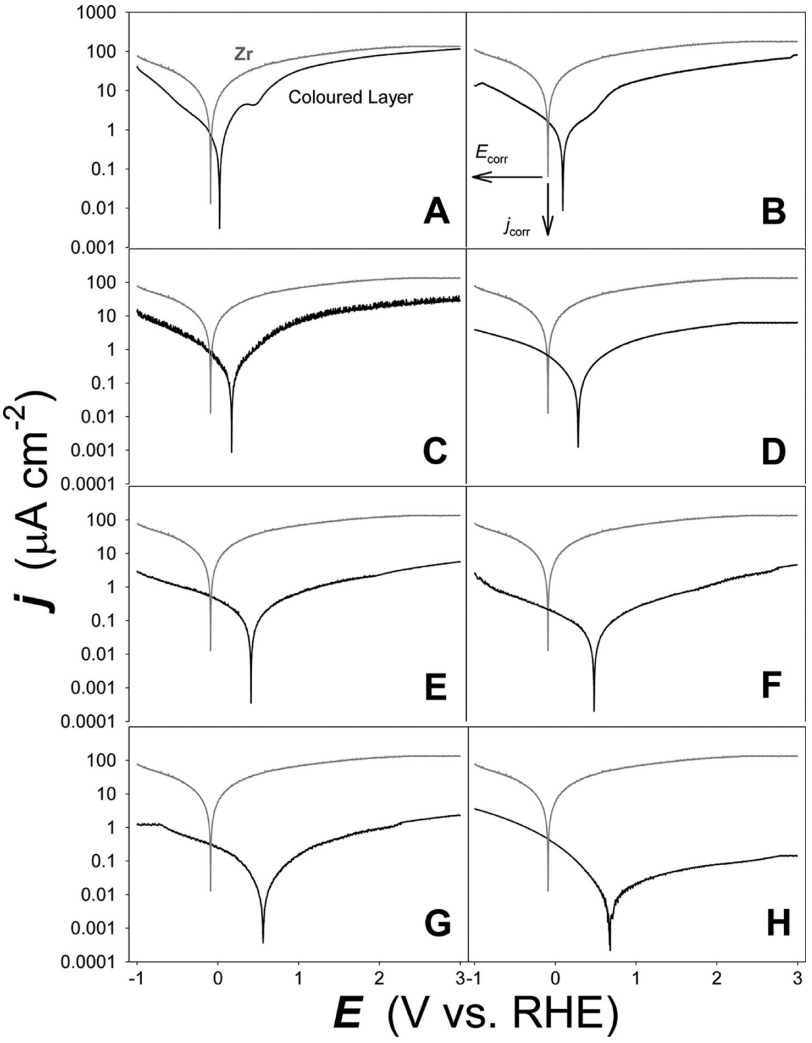

Figure 9. Potentiodynamic polarization curves recorded in 1 wt % aqueous NaCl solution in the potential range from −1.0 to +3.0 V at a scan rate of s = 1 mV s^{-1} and at a temperature of T = 298 K. The graphs A−H present two polarization curves, one for etched and nonpassivated Zr (gray line) and the other for a colored layer formed at a given V_{ac} (black line). Graph B presents the approach applied to the determination of E_{corr} and j_{corr}.

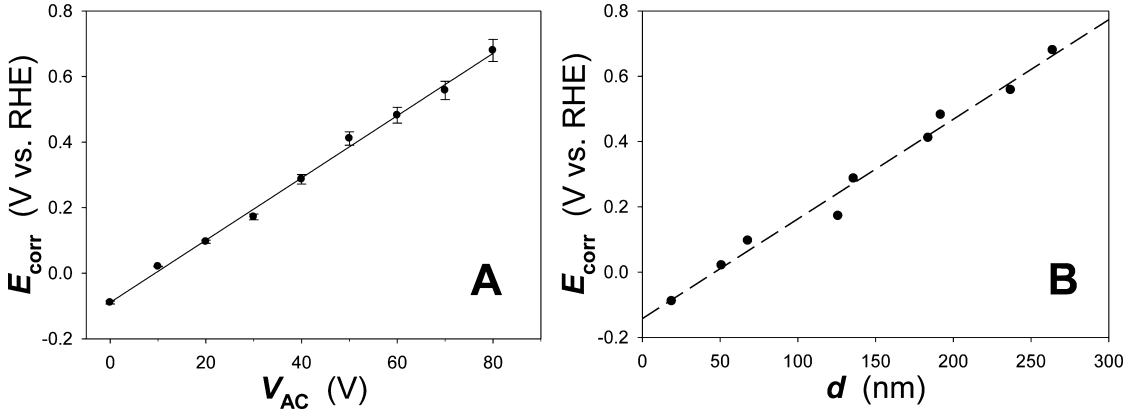

Figure 10. Graph A: the relationship between E_{corr} and V_{ac}. Graph B: the relationship between E_{corr} and d. Both graphs refer to the colored passive layers formed on etched Zr.

passivated Zr; (iv) at any given E, the value of j decreases with an increase in V_{ac}, thus with an increase in thickness of the colored passive layer; and (v) the development of a colored passive layer increases the corrosion potential (E_{corr}) and decreases the corrosion current density (j_{corr}) as compared to etched and nonpassivated Zr; in other words, etched Zr covered with a colored passive layer is more stable than nonpassivated Zr. In order to advance the analysis of corrosion behavior of the colored passive layers on etched Zr, we determined the values of E_{corr} and j_{corr} (graph B in Figure 9 presents the approach applied to the determination of E_{corr} and j_{corr}). The graph A in Figure 10 shows the variation of E_{corr} with

dx.doi.org/10.1021/am301389u | ACS Appl. Mater. Interfaces 2012, 4, 6487−6498

V_{ac} and reveals that the formation of progressively thicker passive layers increases E_{corr} linearly from −0.09 V for nonpassivated Zr to +0.68 V for the colored passive layer formed at V_{ac} = 80 V. Figure 5 in the section Ion Beam and Electron Microscopy Characterization presents the thickness of the colored passive layers as a function of V_{ac} and shows that d increases linearly with V_{ac}. Because there is also a linear relationship between E_{corr} and V_{ac}, we expect that there should be a linear relationship between E_{corr} and d. The graph B in Figure 10 demonstrates that, indeed, E_{corr} increases linearly with d, thus proving that the thicker the colored passive layer on etched Zr, the greater its corrosion resistance. Figure 11

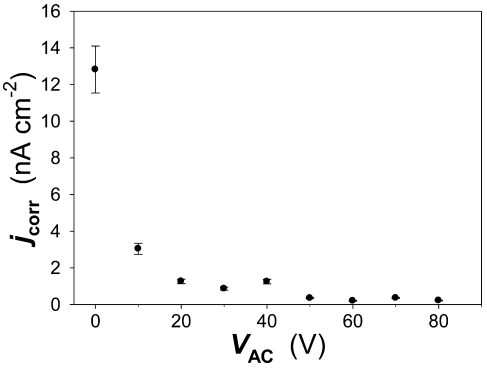

Figure 11. Relationship between j_{corr} and V_{ac} for the colored passive layers formed on etched Zr.

presents a relationship between j_{corr} and V_{ac} and demonstrates that the values of j_{corr} are very small and decrease from 12.8 nA cm^{-2} for etched and nonpassivated Zr to 0.2 nA cm^{-2} for the colored passive layer formed at V_{ac} = 80 V. Formation of the thinnest colored passive layer by the application of V_{ac} = 10 V (d = 51 nm) already reduces j_{corr} to 3 nA cm^{-2}, thus by a factor of 4 as compared to nonpassivated Zr. As V_{ac} is further increased, j_{corr} decreases even more but the change in its magnitude is progressively less due to the exponential decrease of j_{corr} with increasing V_{ac}. It is interesting to observe that although the VLM and AFM results (Figures 1 and 2) reveal the presence of surface defects in the colored passive layers on Zr, they do not affect their corrosion behavior.[35] This observation suggests that either the defects are inactive in corrosion reactions or that their corrosion rate is similar to that of the surrounding material.[34,36−38] The defects cannot be related to pitting corrosion because an inspection of the Zr samples by VLM after prolonged exposure to 1 wt % aqueous NaCl solution did not reveal any changes in their size or structure.

CONCLUSIONS

In summary, zirconium can be successfully colored by the application of ac voltage in an aqueous solution of Na_2SO_4. Such formed colored passive layers reveal a broad range of bright, uniform, and well-defined colors that originate from iridescence. Their coloration can be fine-tuned by adjusting the applied ac voltage, and the procedure is relatively simple and scalable. Analysis of the surface morphology of the colored passive layers on Zr using visible light microscopy, and atomic force microscopy reveals that they are compact and free of surface fractures, although they possess microscopic pore-like surface defects. The surface topography of the colored passive layer can be examined in the micrometer and nanometer ranges using stylus surface profilometry and atomic force microscopy, respectively. The profilometry results reveal that microroughness of the colored passive layers is lower than that of nonpassivated Zr. On the other hand, atomic force microscopy data show there are hardly any changes in the nanoroughness upon the development of the colored passive layers. The application of reflectance spectroscopy allows identification of spectral regions in the visible range that contribute to the resultant coloration as detected by visual inspection. In most cases, the coloration originates from two or three contributing colors. This observation is corroborated by the results of visible light microscopy analysis, which show that different grains have different colors. Focused ion beam combined with scanning and transmission electron microscopies is instrumental in determination of the thickness of the colored passive layers and in examination of their crystallographic structure. Their thickness is found to increase linearly with increasing the ac voltage required to form them. The electron microscopy results also indicate that the colored passive layers are crystalline in nature. Evaluation of the corrosion behavior of the colored passive layers in 1 wt % aqueous NaCl solution is carried out using inductively coupled plasma-mass spectrometry that quantifies the amount of Zr in the electrolyte and electrochemical techniques that determine the corrosion potential and current density. The polished Zr samples, whether colored or not, reveal an outstanding stability in the aqueous NaCl solution. On the other hand the stability of the etched Zr samples is significantly lower than that of Zr but the formation of colored passive layers improves their corrosion resistance. The inductively coupled plasma-mass spectrometry results are supported by the electrochemical measurements, which demonstrate that the formation of colored passive layers on Zr increases the corrosion potential and decreases the corrosion current density, and in general the thicker the colored passive layer the higher its corrosion potential and the lower its current density.

Our electrochemical method of passivating Zr has shown itself to be an excellent procedure for future scalable applications in industry, without relying on temporary paints and adhesives for coloration. Through the reduction in corrosion offered by the passive layers, Zr will be able to be employed as an alternative to Ti in many applications where a smoother chemically etched surface is required or a variation in color is desired. This reduction in corrosion will also increase the longevity of Zr in its current applications in nuclear, chemical, and aesthetic (jewelry) industries as well as in biomedical implants and devices,[39−41] electronic devices,[42] structural materials, and large scale construction equipment.[32]

AUTHOR INFORMATION

Corresponding Author

*E-mail: gregory.jerkiewicz@chem.queensu.ca (G.J.); diane.beauchemin@chem.queensu.ca (D.B.).

Notes

The authors declare no competing financial interest.

ACKNOWLEDGMENTS

We gratefully acknowledge financial support towards this project from the NSERC of Canada (Discovery Grant and Research Tools and Instruments Grants). We gratefully acknowledge collaboration with the Application Laboratory of

Carl Zeiss NTS Division in Oberkochen, Germany, and access to their materials characterization facilities.

REFERENCES

(1) Miller, G. L. *Metallurgy of the Rarer Metals − 2 Zirconium*; Butterworths Scientific Publications: London, 1954.
(2) Petit, J. A.; Chatainier, G.; Dabosi, F. *Corros. Sci.* **1981**, *21* (4), 279−299.
(3) Askeland, D. R.; Phulé, P. P. *The Science and Engineering of Materials*, 5th ed.; Nelson: Toronto, Canada, 2006.
(4) Hayes, E. T. *Zirconium: Its Production and Properties*; United States Government Printing Office: Washington, DC, 1956.
(5) Schlechten, A. W. *Rare Metals Handbook*; Reinhold Publishing Corp.: New York, 1954.
(6) Jones, D. A. *Principles and Prevention of Corrosion*; Macmillan Pub. Co.: New York, 1992.
(7) Mogoda, A. S. *Thin Solid Films* **1999**, *357*, 202−207.
(8) Wang, L.-N.; Luo, J.-L. *Electrochem. Commun.* **2010**, *12* (11), 1559−1562.
(9) Yau, T. L. *Corrosion and Corrosion Protection Handbook−Zirconium*, 2nd ed.; Marcel Dekker Inc.: New York, 1989.
(10) Han, Y.; Zhang, L.; Lu, J.; Zhang, W. *J. Mater. Res.* **2009**, *24* (10), 3136−3245.
(11) Rosalbino, F.; Maccio, D.; Saccone, A.; Angelini, E.; Delfino, S. *J. Solid State Electrochem.* **2010**, *14* (8), 1451−1455.
(12) Wyszecki, G.; Styles, W. S. *Color Science: Concepts and Methods, Quantitative Data and Formulae*; Wiley-Interscience: New York, 1982.
(13) Nassau, K. *The Physics and Chemistry of Colors*; Wiley-Interscience: New York, 1983.
(14) Fairchild, M. *Colour Appearance Models*; Addison-Wesley: Reading, MA, 1998.
(15) Jerkiewicz, G.; Strzelecki, H.; Wieckowski, A. *Langmuir* **1996**, *12*, 1005−1010.
(16) Hrapovic, S.; Luan, B. L.; D'Amours, M.; Vatankhah, G.; Jerkiewicz, G. *Langmuir* **2001**, *17*, 3051−3060.
(17) Zhao, J.; Xu, R.; Wang, X.; Li, Y. *Corros. Sci.* **2008**, *50* (6), 1593−1597.
(18) Charlesby, A. *Acta Metall.* **1953**, *1*, 340−347.
(19) Zhao, B.; Jerkiewicz, G.; Hrapovic, S.; Luan, B. *Chem. Mater.* **2008**, *20*, 1877−1880.
(20) Burgers, W. G.; Claasen, A.; Zernicke, I. *Z. Phys. A: Hadrons Nucl.* **1932**, *74*, 593−603.
(21) Bolduc, S. Master's Thesis, Queen's University, Kingston, Ontario, Canada, 2003.
(22) Huang, Y. Z.; Blackwood, D. J. *Electrochim. Acta* **2005**, *51* (6), 1099−1107.
(23) di Quarto, F.; Doblhofer, K.; Gerischer, H. *Electrochim. Acta* **1978**, *23*, 195−201.
(24) Sul, Y.-T.; Johansson, C. B.; Petronis, S.; Krozer, A.; Jeong, Y.; Wennerberg, A.; Albrektsson, T. *Biomaterials* **2002**, *23*, 491−501.
(25) Zhao, B. Ph.D. Thesis, Queen's University, Kingston, Ontario, Canada, 2007.
(26) Lausmaa, J. In *Titanium in Medicine: Material Science, Surface Science, Engineering, Biological Responses, and Medical Applications*; Brunette, D. M., Tengvall, P., Thomsen, P., Textor, M., Eds.; Springer: New York, 2001.
(27) Munro, A. Master's Thesis, Queen's University, Kingston, Ontario, Canada, 2006.
(28) Munro, A.; Cunningham, M. F.; Jerkiewicz, G. *ACS Appl. Mater. Interfaces* **2010**, *2* (3), 854−862.
(29) Munro, A.; Cunningham, M. F.; Jerkiewicz, G. *ACS Appl. Mater. . Interfaces* **2011**, *2* (4), 1195−1203.
(30) Zhao, B.; Jerkiewicz, G. *Can. J. Chem.* **2006**, *84*, 1132−1145.
(31) Mogoda, A. S. *Corrosion* **1999**, *55* (9), 877−882.
(32) Hackerman, N.; Cecil, O. B. *J. Electrochem. Soc.* **1954**, *101*, 419−425.
(33) Maraghini, M.; Adams, G. B.; Van Rysselberghe, P. *J. Electrochem. Soc.* **1955**, *101*, 400−409.
(34) Oliveira, N. T. C.; Biaggio, S. R.; Rocha-Filho, R. C.; Bocchi, N. *J. Braz. Chem. Soc.* **2002**, *13* (4), 463−468.
(35) Archibald, L. C.; Leach, J. S. L. *Electrochim. Acta* **1977**, *22*, 15−20.
(36) Petit, J. A.; Chatainier, G.; Dabosi, F. *Corros. Sci.* **1981**, *21* (4), 279−299.
(37) Anisimov, M. P. *Russ. Chem. Rev.* **2003**, *72* (7), 591−628.
(38) Kobayashi, E.; Matsumoto, S.; Yoneyama, T.; Hamanaka, H. *J. Biomed. Mater. Res.* **1995**, *29*, 943−950.
(39) Lee, D. B.; Roberts, M.; Bluchel, C. G.; Odell, R. A. *ASAIO J.* **2010**, *56* (6), 550−556.
(40) Wang, L.-N.; Luo, J.-L. *J. Phys. D: Appl. Phys.* **2011**, *44*, 075301−075309.
(41) Gomez Sanchez, A.; Schreiner, W.; Duffo, G.; Cere, S. *Appl. Surf. Sci.* **2011**, *257* (15), 6397−6405.
(42) Cabral, C. Jr.; Callegari, A. C.; Gribelyuk, M. A.; Jamison, P. C.; Lacey, D. L.; McFeely, F. R.; Narayanan, V.; Neumayer, D. A.; Ranade, P.; Zafar, S. *Deposition of hafnium oxide and/or zirconium oxide and fabrication of passivated electronic structures*. U.S. Patent 7,566,938, July 28, 2009.